Sensing of acetone by Al-doped ZnO

Ran Yoo[a], Andreas T. Güntner[b], Yunji Park[a], Hyun Jun Rim[a], Hyun-Sook Lee[a], Wooyoung Lee[a],[*]

[a] *Department of Materials Science and Engineering, Yonsei University, 50 Yonsei-ro, Seodaemun-gu, Seoul, 03722, Republic of Korea*
[b] *Particle Technology Laboratory, Department of Mechanical and Process Engineering, ETH Zürich, Sonneggstrasse 3, 8092, Zürich, Switzerland*

ARTICLE INFO

ABSTRACT

The development of chemoresistive gas sensors for environmental and industrial air monitoring as well as medical breath analysis is investigated. Flame-made ZnO nanoparticles (NPs) doped with 1 at% Aluminum exhibited higher sensing performance (*response* 245, response time ∼ 3 s, and *sensitivity* 23 ppm^{-1}) than pure ZnO and those made by a hydrothermal method (HT) (56, ∼ 12 s, and 4 ppm^{-1}) for detection of 10 ppm acetone. Furthermore, their sensing response of ∼10 to 0.1 ppm of acetone at 90% RH is superior to other metal oxide sensors and they feature good acetone selectivity to other compounds (including NH_3, isoprene and CO). Characterization by N_2 adsorption, X-ray photoelectron and UV–vis spectroscopies reveals that the improved sensing performance of flame-made Al-doped ZnO NPs is associated primarily to a higher density of oxygen vacancies than pure ZnO and all HT-made NPs. This leads to a greater number of adsorbed oxygen ions on the surfaces of Al-doped ZnO NPs, which can react with acetone molecules.

1. Introduction

Exhaled breath is a source of potential biomarkers for the detection of certain diseases. Endogenous inorganic gases e.g., NO and CO and volatile organic compounds (VOCs) e.g. acetone, ethanol, ammonia, ethane and pentane in the human breath, serve as such biomarkers for several diseases [1]. Acetone, a volatile metabolic by-product of lipolysis [2], can be found at elevated concentration in the exhaled breath of uncontrolled diabetics [3] and subjects with enhanced fat metabolism, e.g. during/after fasting [4] and exercise [5]. Typical breath acetone concentrations of healthy humans range from 0.3 to 4 ppm [6,7] while can increase up to 40 ppm in adults following a ketogenic diet (consuming low carbohydrates and high fat) [8].

Breath acetone concentration has been measured by gas chromatography (GC) [9], selected ion flow tube mass spectrometry (SIFT-MS) [10], ion mobility spectrometry (IMS) [11], and proton transfer reaction mass spectrometry (PTR-MS) [12]. However, these technologies are often complex, rather bulky and expensive; thus, hardly suitable as portable detectors for widespread application. Chemical sensors are promising for their compact design [13], high sensitivity, low cost, integration into portable analyzers [14] and ready application in breath acetone detection [5]. Indeed, several reports introduced chemoresistive sensors based on ε-WO$_3$ [15], SnO$_2$ [16], Co$_3$O$_4$ [17], ZnO [18], ZnO/ZnFe$_2$O$_4$ [19], In-loaded WO$_3$/SnO$_2$ [20] and Ag-ZnO-loaded graphitic CN [21] that have been explored for detection of acetone

while other VOCs (e.g. ethanol [22]) can be detected as well. Among them ZnO is quite attractive for its relatively simple preparation, high chemical and thermal stability [23], especially when doped, for instance, with Ti [24], having covalent/ionic aspects in its chemical structure, high sensitivity, low response and recovery time [25], and sensitivity to VOCs and combustible gases [26]. The sensing properties of ZnO can be modulated by its particle morphology, crystal structure, energy band structure and number of surface sites available for gas interaction [27]. Doping ZnO with aliovalent metal has been proven to be an effective technique for altering the electronic structure of ZnO. For instance, the addition of Ti during flame aerosol synthesis of ZnO turned it isoprene-selective [24]. Furthermore, we recently demonstrated a sensor based on Al-doped ZnO nanoparticles (NPs) synthesized by a hydrothermal method (HT), which exhibited high sensitivity for acetone (see supplementary).

Here we report the effect of Al dopant on the nanostructure, optical, and gas sensing properties of ZnO NPs for acetone detection. The metal-oxide NPs are made by flame spray pyrolysis (FSP) featuring superior control over material composition and morphology (e.g. particle & crystal size, shape) by combustion of liquid precursors [28]. For fabrication of pure and doped ZnO, hydrothermal methods possess some advantages including low synthesis temperature, simple equipment, usually cheap and environmentally friendly chemicals, and good quality of crystals [29]. On the other hand, FSP is a proven scalable [30] dry deposition technique to pattern highly porous sensing films

---

* Corresponding author.
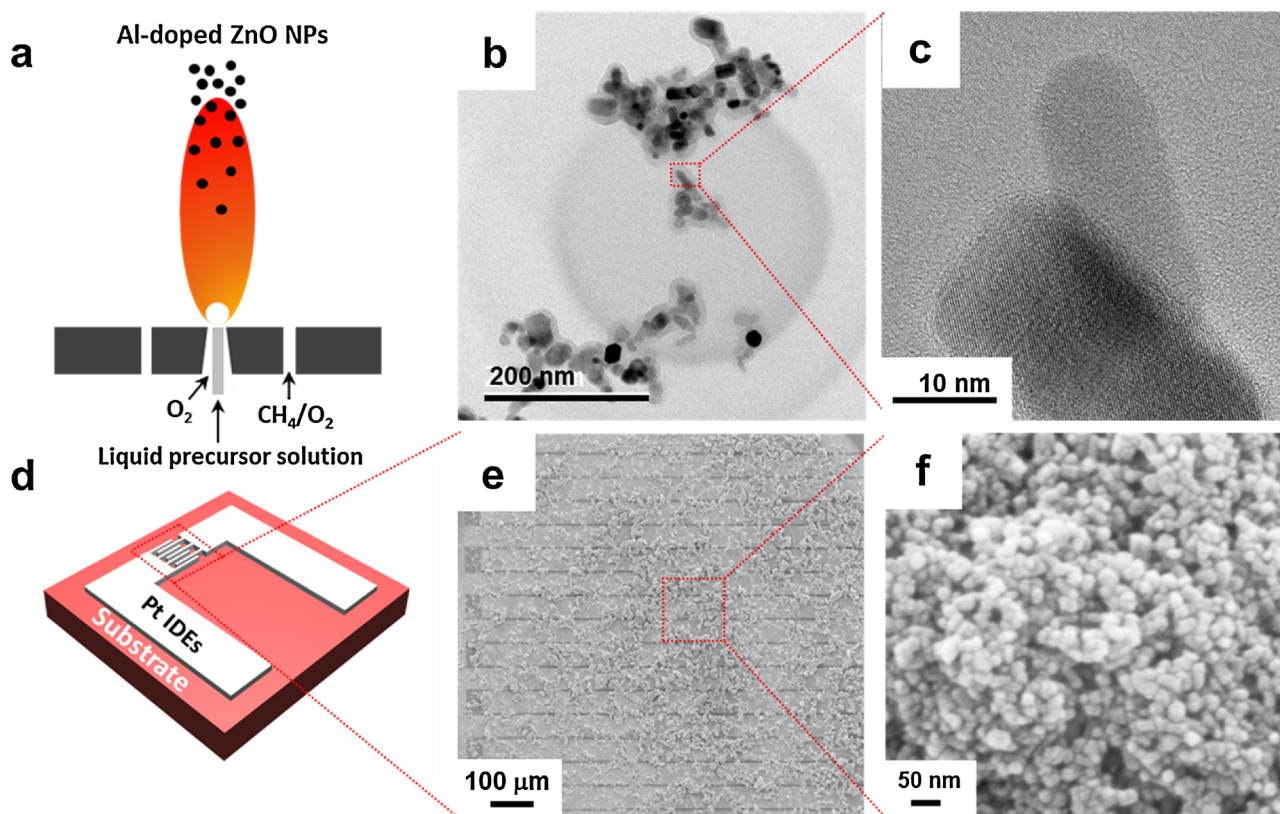 *E-mail address:* wooyoung@yonsei.ac.kr (W. Lee).

Fig. 1. (a) Schematic of FSP synthesis of Al-doped ZnO NPs, (b) TEM image of the filter-collected, as-prepared NPs, (c) HRTEM image of isolated NPs, (d) schematic of the sensor device, (e) SEM image of the sensing film on top of the interdigitated Pt electrodes after annealing with its magnification shown in (f).

onto entire wafers [31]. Most remarkably, it features wide flexibility to tune material composition with superior control over particle size [32] and high purity due to the gas phase conversion. That way, novel sensing materials based on solid solutions (e.g. Ti-doped ZnO [24]), mixed oxides (e.g. SiO_2/MoO_3 [33]) and even metastable phases (e.g. ε-WO_3 [18]) have can be captured exhibiting unique sensing properties that has led also to the creation of nearly orthogonal sensor arrays [34]. The sensing performance of FSP-made pure and Al-doped ZnO NPs is closely compared to HT-made NPs. Finally, the surface elemental states, band gaps and specific surface areas are investigated along with the number of oxygen vacancies in the ZnO made by both FSP and HT by N_2 adsorption, X-ray photoelectron and UV–vis spectroscopies and compared to the electrical conductivity and sensing performance.

2. Materials and methods

Pure and Al-doped ZnO NPs were made by a FSP reactor, (see Fig. 1a) described in detail elsewhere [35]. The precursor solutions consisted of zinc 2-ethylhexanoate (Strem chemicals, purity > 99%, 22 wt.% Zn) diluted in xylene (Sigma Aldrich, purity methanol ≥ 96%). For the synthesis of Al-doped ZnO NPs, aluminum acetyl-acetonate (Al $(C_5H_7O_2)_3$, Sigma Aldrich, purity 99%) was added to achieve an atomic concentration of 1.0%. The overall constant metal ion concentration (Zn + Al) was 0.5 mol L^{-1}. The precursor solution was supplied at 5 mL min^{-1} through the FSP nozzle and dispersed by 5 L min^{-1} oxygen (pressure drop 1.5 bar) into a fine spray. The dispersed precursor solution was ignited by a ring-shaped flame consisting of premixed methane/oxygen (1.22/3.25 L min^{-1}). The produced NPs were collected on a glass fiber filter (GF6 Albet-Hahnemuehle, 257 mm diameter) placed 50 cm above the burner (HAB) using a vacuum pump (Seco SV 1025 C, Busch, Switzerland).

Sensor devices based on ZnO NPs were fabricated according to the

procedure described in our previous report [36]. The NPs were mixed with α-terpineol to form a paste and dispersed onto interdigitated Pt electrodes using a dropping method. The devices were subsequently dried at 300 °C for 1 h and annealed at 600 °C for another hour to remove the solvent and enhance the thermal and mechanical stability of ZnO NPs.

The shape and morphology of the as-prepared ZnO NPs were probed by a field-emission scanning electron microscope (FE-SEM; JEOL 7001 F). Their crystal structure and microstructure were characterized by X-ray diffraction (XRD, Ultima IV/ME 200DX, Rigaku) with Cu Kα radiation and transmission electron microscopy (TEM, JEOL JEM ARM 200 F), respectively. Lanthanum hexaboride (LaB_6) was used as an internal standard for the XRD analysis. Surface elemental analysis was performed by X-ray photoelectron spectroscopy (XPS, K-alpha Thermo VG) using Al Kα radiation (1486.6 eV) from an X-ray source operated at 12 kV with a current of 3 mA. The optical properties of the ZnO NPs were examined using a UV–vis spectrophotometer (UV–vis, V-650 JASCO) in the wavelength range of 250–800 nm. N_2 adsorption-desorption analysis was carried out to measure the Brunauer-Emmett-Teller (BET) specific surface area of the NPs. The specific surface areas of the NPs were calculated from the N_2 adsorption isotherms (Autosorb-iQ2ST/MP Quantachrome).

Sensing measurements were conducted at 250–500 °C using a gas detecting system [37]. The flow of a mixture of acetone gas and air was controlled by mass flow controllers (MFCs). The sensing properties were measured using a combination of a current source (Keithley 6220) and a nanovoltmeter (Keithley 2182) with a constant current supply of 10 nA for a time interval of 1 s. The sensing response for acetone was calculated as: *Response* $= (R_{air} - R_{gas})/R_{gas}$, where R_{gas} and R_{air} are the resistances of the sensors in air with and without acetone, respectively. The response time is defined as a time required to reach 90% of the total resistance change upon the exposure to the test gas.
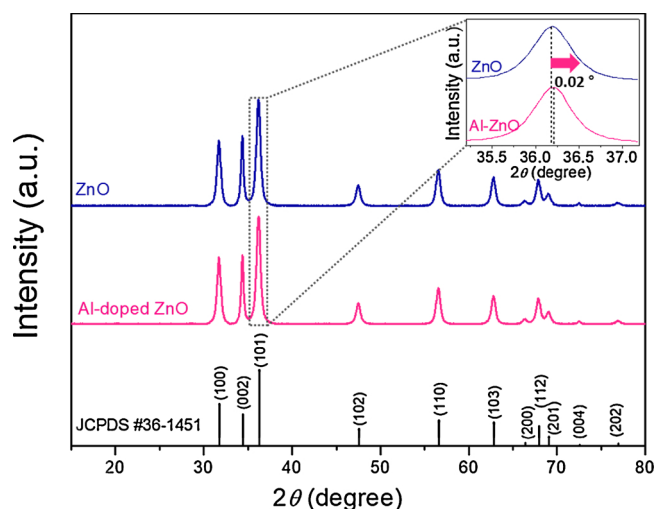
Fig. 2. XRD patterns of the pure and Al-doped ZnO NPs made by FSP. The black bars at the bottom are for reference and correspond to hexagonal wurtzite-type ZnO (JCPDS #36-1451). The inset shows the magnified (101) peak.

3. Results and discussion

Fig. 1a schematically illustrates the synthesis of Al-doped ZnO NPs by FSP from a liquid organometallic precursor solution. The Al-doped

ZnO NPs are formed by nucleation and subsequent coagulation, aggregation and agglomeration and collected by filtration [38]. Aluminum cations are probably incorporated into the ZnO lattice of the NPs during their nucleation. Figs. 1b,c show TEM images of these NPs. Fig. 1b and its magnification (Fig. 1c) suggest that the shapes of NPs are irregular, from rather spherical to rod-like. This is similar to FSP-made pure ZnO [39] while HT synthesis resulted in rather spherical NPs at identical Al-doping concentration (see supplementary). Furthermore, the average NP size is in the range of 10–30 nm. Fig. 1d presents a schematic of a sensor device (8.5 mm × 8.5 mm) fabricated by deposition of interdigitated Pt electrodes (5 µm spacing) onto a Si/SiO$_2$ substrate. The SEM image of the deposited sensing film after drying and annealing is shown in Fig. 1e with its magnification in Fig. 1f. The NPs seem to be nearly spherical. The rod-like ones probably converted into larger spherical particles during annealing, consistent with Ti-doped ZnO [24].

Fig. 2 shows the XRD patterns of FSP-made pure and Al-doped ZnO NPs. All patterns indicate that the ZnO NPs formed a hexagonal wurtzite phase (JCPDS #36-1451), in line with previous studies on pure ZnO even at other precursor and flame conditions [39]. No other secondary crystalline phases or impurities could be observed. The main (101) peak position in the Al-doped samples was observed to shift slightly to larger angles compared to that in pure ZnO NPs (inset of Fig. 2). This shift was about 0.02° for the Al-doped ZnO NPs synthesized by FSP. It is attributed to the reduction in the interlayer spacing of ZnO along the (101) axis by replacing Zn^{2+} (0.74 Å) with smaller Al^{3+} ions (0.53 Å) [40] in the ZnO lattice. This shift was larger (~0.04°) for HT-made Al-doped
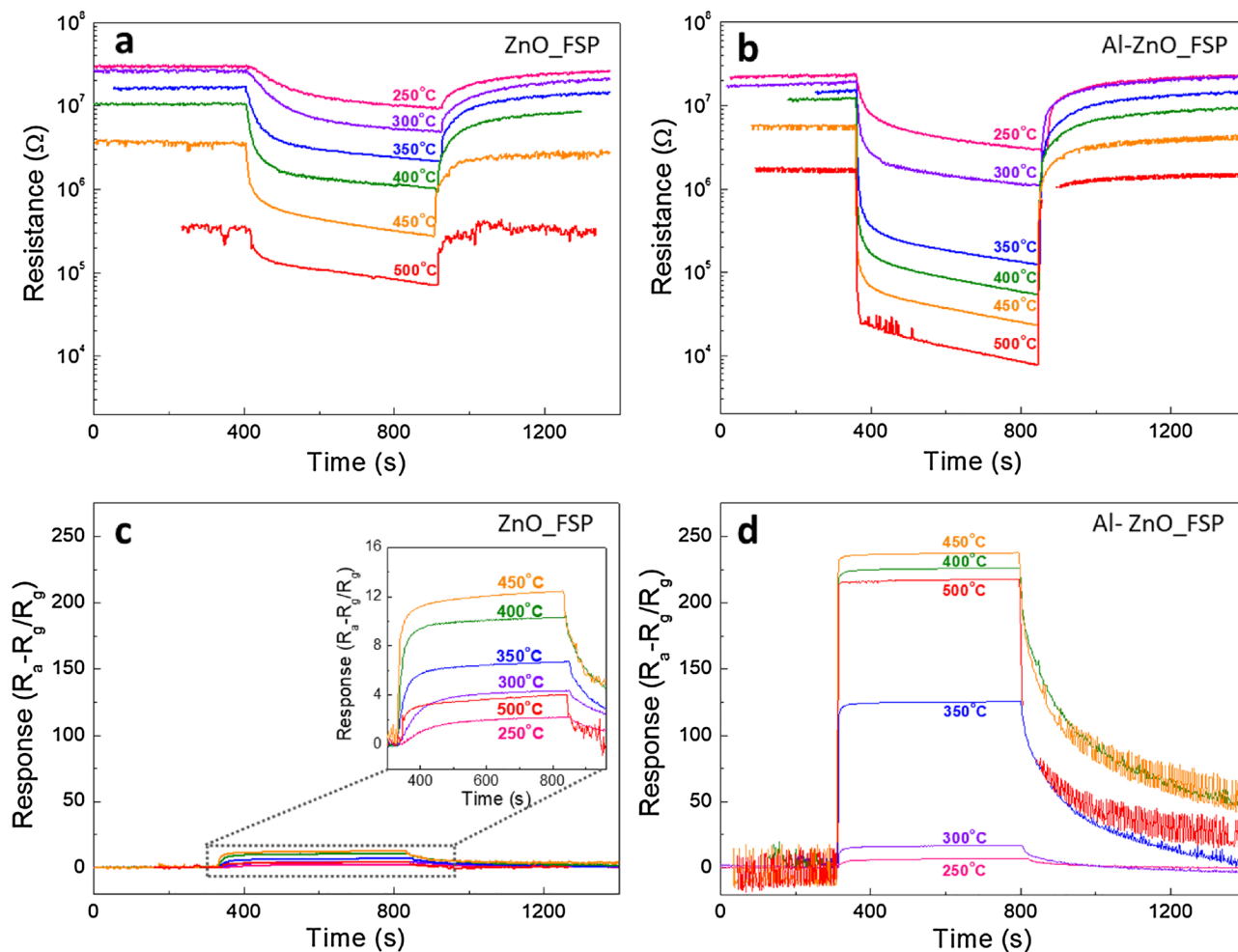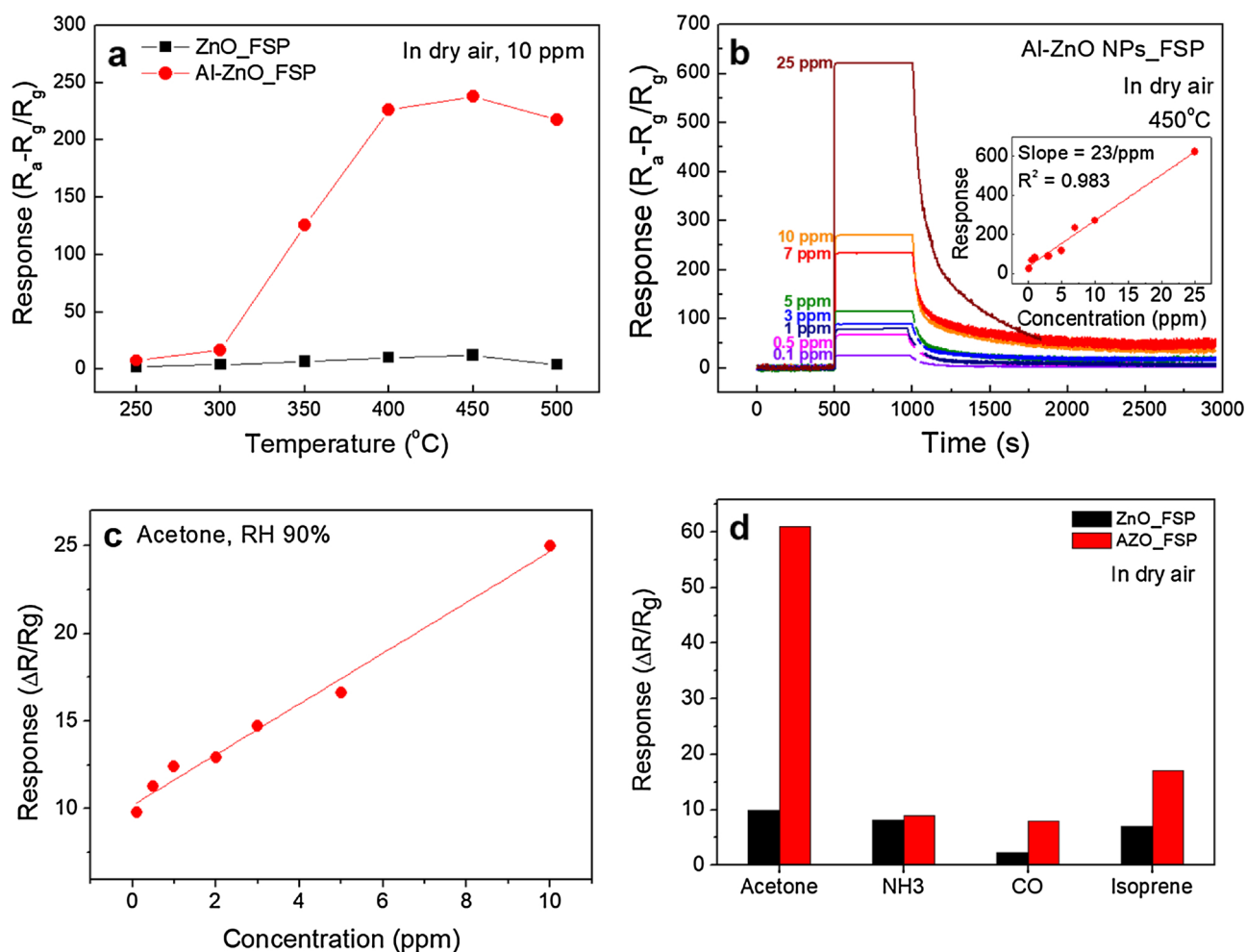

Fig. 3. Variations in the resistance (a, b) and sensing response (c,d) of pure and Al-doped ZnO NPs, respectively, upon exposure to 10 ppm of acetone in the operating temperature range of 250–500 °C. The inset in (c) shows the magnified sensor responses.

Fig. 4. (a) Sensor response of the pure (squares) and Al-doped (circles) ZnO NPs fabricated by FSP at 10 ppm acetone as a function of operating temperature. (b) Sensing response of Al-ZnO NPs at an optimum operating temperature of 450 °C as a function of acetone concentration. The inset shows the sensitivity calculated from a linear fit of the responses. (c) The sensing response of the Al-doped ZnO NPs as a function of acetone concentration under 90% relative humidity (RH). (d) The sensing response of the Al-doped ZnO NPs for breath-relevant acetone, NH_3, Isoprene and CO at 1 ppm in dry air.

ZnO NPs at same nominal composition (see supplementary), The smaller lattice distortion of FSP-made Al-doped ZnO should indicate that less Al is incorporated into the ZnO lattice. This could mean that some Al is at the surface, as observed for Ti-doped ZnO [24].

The sensing properties of pure and Al-doped ZnO NPs were measured on exposure to 10 ppm of acetone at different operating temperatures. As can been seen in Fig. 3, the variations in the resistance and sensing response by pure and Al-doped ZnO were observed at 250–500 °C. As shown in Fig. 3a,b, the initial resistance of pure and Al-doped ZnO decreases with increasing temperature. This is attributed to the intrinsic properties of semiconducting metal oxides. As shown in Fig. 3c,d, the sensing responses of pure and Al-doped ZnO NPs to acetone strongly depend on the operating temperature. The response increases with increasing temperature up to 450 °C and then decreases at 500 °C. The low response at 500 °C can be attributed to desorption of chemisorbed oxygen from the surface of ZnO NPs [41]. All tested ZnO NPs exhibited the maximum response also at 450 °C.

An overview of the sensing response of FSP-made Al-doped ZnO NPs is displayed in Fig. 4. The maximum sensing responses of pure and Al-doped ZnO NPs upon exposure to 10 ppm acetone (Fig. 3) are plotted as a function of operating temperature (Fig. 4a). Most importantly, Al-doped ZnO NPs exhibit much higher responses than pure ZnO at 200–500 °C. Highest responses were obtained at 450 °C being ~13 and ~245 for pure and Al-doped ZnO, respectively.

The sensitivity of Al-doped ZnO was measured at the optimum working temperature of 450 °C in the acetone concentration range from 0.1 to 25 ppm. The response changes at different acetone concentrations are displayed in Fig. 4b. The inset of Fig. 4b shows the corresponding responses. At 0.1 ppm, the Al-doped ZnO exhibits a response of ~25 at a signal-to-noise ratio of 5. The response increased rather linearly when the acetone concentration varied from 0.1 to 25 ppm with a sensitivity of approximately 23 ppm^{-1} (correlation coefficient $R^2 = 0.983$).

In human breath, some analytes are present at high ppb or even ppm level (e.g., isoprene, NH_3, or CO) [42] and high relative humidity (RH, ~89 - 97%) [43]. Fig. 4c presents the sensing response as a function of acetone concentration at 90% RH. The sensing responses are ~10 at 0.1 ppm and ~25 at 10 ppm, respectively. Relevant sensing properties (sensing response, low detection limit and response time) of the Al-doped ZnO NPs under a humid condition (RH 90%) are shown and benchmarked to state-of-the-art chemoresistive acetone sensors in Table 1 [44–47]. The FSP-made Al-doped ZnO features the highest response to 1 ppm of acetone at 90% RH, while the lowest measured concentration and response time are attractivefor breath analysis.

Fig. 4d shows the response of the Al-doped ZnO NPs to 1 ppm of acetone, isoprene, NH_3, and CO at 450 °C in dry air. The Al-doped ZnO NPs show high acetone selectivity to NH_3, isoprene, and CO with response ratios of 6.9, 3.6 and 7.4, respectively. This is superior to pure

Table 1
Summary of sensing properties of state-of-the-art chemoresistive acetone sensors.

	[36]	[37]	[38]	[39]	This work
Materials	Si:WO$_3$	NOGR-H-WO$_3$	Rh-WO$_3$	SnO$_2$ + RGO	Al-ZnO
Synthesis	FSP	Electrospinning	Spray pyrolysis	Electrospinning	FSP
Response	1.27	7.6	3	3.5	10
	(0.5 ppm, RH 90 %)	(1 ppm, RH 90 %)	(1 ppm, RH 80 %)	(1 ppm, RH 90 %)	(1 ppm, RH 90 %)
Lowest measured concentration	0.02 ppm	1 ppm	0.2 ppm	1 ppm	0.1 ppm
Response time	< 15 s	15 s	2 s	< 3.3 s	3 s

ZnO that is rather non-specific with quire similar responses to acetone, isoprene and CO. The selectivity of Al-doped ZnO NPs could be preferentially attributed to the much larger dipole moment in the molecular structure of acetone (2.91 D) than that in NH$_3$ (1.42 D), isoprene (0.29 D) and CO (0.122 D). In addition, there are other factors that affect the sensing response such as the analyte's molecular size and molecular weight of gas molecules [48].

Recently Al-doped ZnO NPs synthesized by a hydrothermal method (HT) exhibited high sensing response (*Response* = 56 at 450 °C) to 10 ppm acetone. However, the sensing performance of the Al-doped
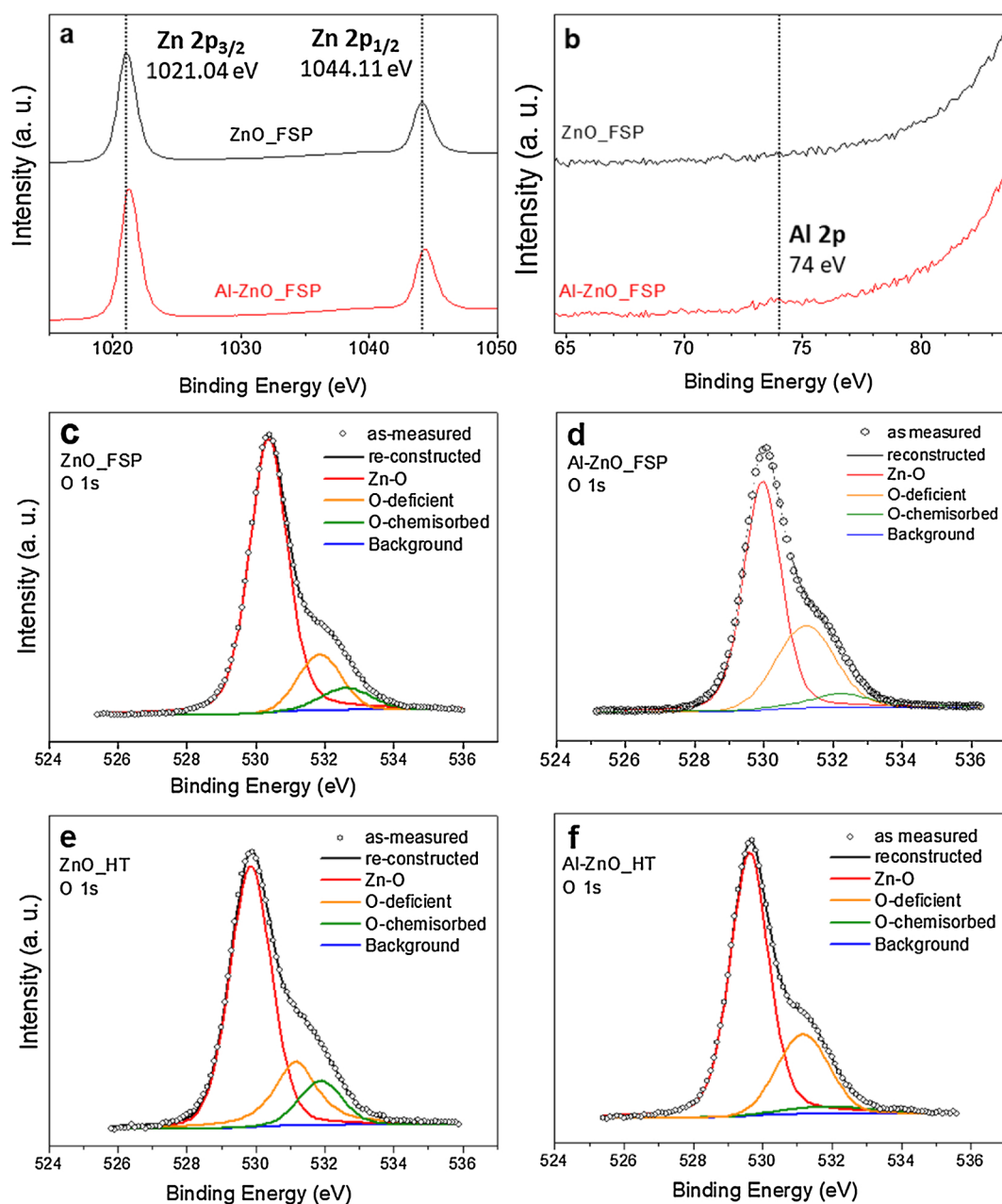
Fig. 5. XPS spectra of (a) Zn 2p and (b) Al 2p of FSP-made ZnO NPs and O 1 s of pure and Al-doped ZnO NPs made by FSP (c,d) and HT (e,f), respectively.
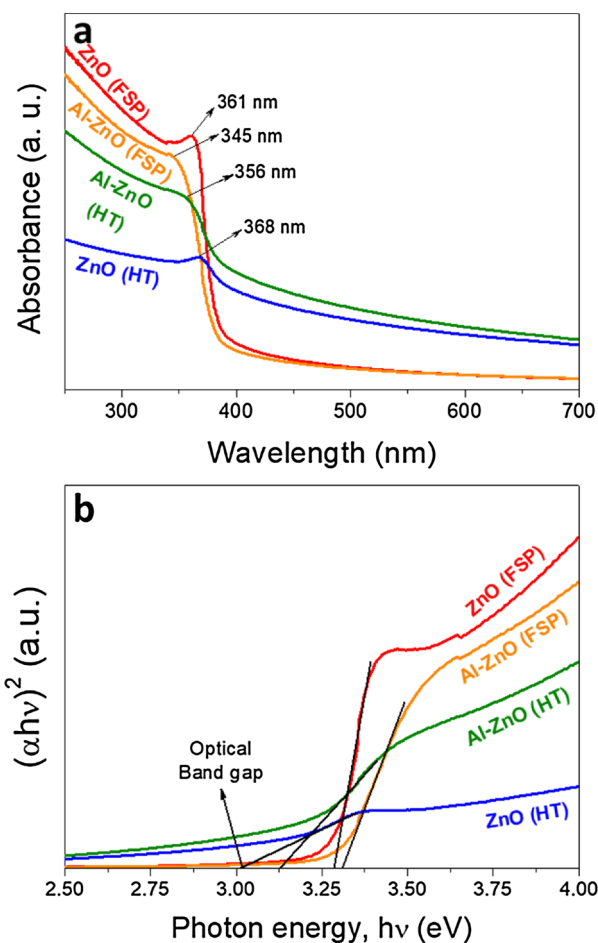
Fig. 6. (a) UV–vis absorption spectra and (b) calculated band gap energies of the pure and Al-doped ZnO NPs synthesized by FSP and HT.

ZnO NPs fabricated by FSP (*Response* = 245 at 450 °C) is much higher than that of HT-made NPs at identical nominal composition. To understand the different sensing performances, we investigated the physical and chemical characteristics, such as oxygen vacancies, band gap, and specific surface area, of pure and Al-doped ZnO NPs made by FSP and HT. An XPS analysis was carried out to investigate the chemical states of pure and Al-doped ZnO made by FSP. Fig. 5 shows the corresponding spectra of Zn 2p (a), Al 2p (b), and O 1 s (c,d). The Zn 2p spectra exhibit two main peaks at 1021.04 and 1044.11 eV which correspond to the Zn $2p_{3/2}$ and Zn $2p_{1/2}$ electronic states, respectively. This indicates the existence of a divalent oxidation state in the ZnO NPs [49]. The Zn 2p spectra of the Al-doped ZnO (red line) display a slight chemical shift compared to pure ZnO (black line) due to the presence of Al atoms in the ZnO structure, indicating the doping effect of Al [50]. The Al 2p spectra (Fig. 5b) show a hump only in the Al-doped ZnO at a binding energy of 74 eV, which is attributed to the Al-O bond. The Al 2p peak at 74 eV is distinguished from metallic Al (~72 eV) or a secondary phase, such as Al_2O_3 (above 75 eV), confirming that Al is incorporated into the Zn^{2+} sites of ZnO [51].

The O 1 s spectra of pure and Al-doped ZnO fabricated by FSP are presented in Fig. 5c and 5d, respectively. The re-constructed O 1 s peaks are deconvoluted into three nearly Gaussian peaks centered at ~529.8, ~531.2, and ~532.1 eV. The 529.8 eV peak (red line) is attributed to the O^{2-} ions of Zn−O bonding in the wurtzite structure of ZnO [50]. The 531.2 eV peak (orange line) is associated with the O^- and O^{2-} ions in the oxygen-deficient regions within the ZnO matrix, whose intensity partly represents the variation in the concentration of oxygen vacancies [51]. The 529.8 eV peak (green line) is related to the chemisorbed oxygen species, such as the adsorbed O_2, H_2O, and CO_2 on the surface of

ZnO [46]. The binding energies of the three peaks are consistent with the Gaussian peaks in a previous report which were centered at ~530.2, 531.1, and 532 eV [52].

The Zn 2 P and Al 2p spectra of pure and Al-doped ZnO NPs made by HT (not shown here) are similar to the corresponding FSP-made ones (Fig. 5a,b). In contrast, the area of the deconvoluted O1 s spectra of the HT-made pure (Fig. 5e) and Al-doped ZnO (Fig. 5f) are smaller than that of the corresponding FSP-made ones. The area fractions of the deconvoluted peaks of pure and doped ZnO NPs, *i.e.*, fractions of oxygen vacancies, were ~21% and ~37% for pure and Al-doped ZnO made by FSP and ~20% and ~25% for pure and Al-doped ZnO made by HT, respectively. As a result, the highest density (37%) of oxygen vacancies was observed for FSP-made Al-doped ZnO that featured also the highest response (R = 245) to 10 ppm of acetone. These results indicate that oxygen vacancies on the surface of ZnO should play an important role for its sensing performance [53].

The electronic structure of pure and Al-doped ZnO NPs were characterized further by UV–vis spectroscopy. In general, UV absorption is related to electronic transitions from the filled valence states to empty conduction states [54]. Fig. 6 presents the UV–vis absorbance spectra (a) and calculated band gap energies (b) of the pure and Al-doped ZnO NPs made by FSP and HT. In the absorption spectra, the peaks at ~361 and ~368 nm for pure ZnO made by FSP and HT, respectively, are blue-shifted to ~345 nm and ~356 nm when doped with Al. Peak shift occurs along with simultaneous peak broadening upon doping with Al which can be explained by the Burstein-Moss (BM) band filling effect [54]. The Fermi level shifts towards the conduction band due to an increase in the electron concentration by Al doping. The optical band gap energy (E_g) can be estimated using the Tauc relation [55]:
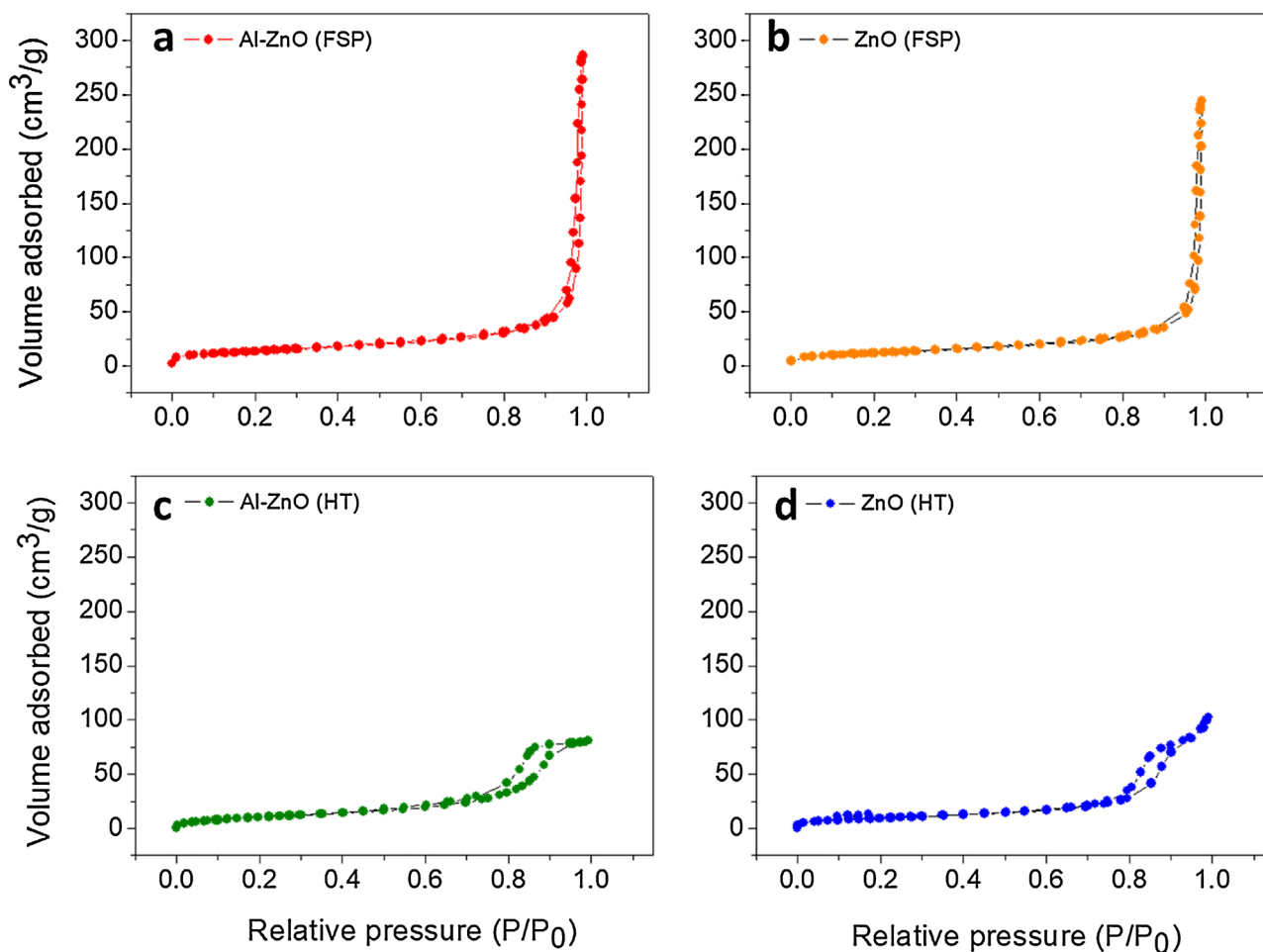
Fig. 7. N$_2$ adsorption-desorption isotherms of the pure and Al-doped ZnO NPs synthesized by FSP and HT.

$$\alpha h\nu = C(h\nu - E_g)^n \tag{1}$$

where α is the absorption coefficient, C is a constant, $h\nu$ is the energy of the incident photons, n = 1/2 for direct band gap semiconductors, and E$_g$ is the optical band gap. The optical band gap energy was calculated by extrapolating the function $[F(\alpha h\nu)^2]$ versus $h\nu$ to zero as suggested by Weber [56]; the results of the extrapolation are shown in Fig. 6b. The optical band gaps of the Al-doped compared to the pure ZnO NPs fabricated by HT and FSP, increased from 3.02 and 3.28 eV to 3.13 and 3.31 eV, respectively. Such phenomena are attributed to the shift in the Fermi level towards the conduction band, caused by additional carriers from donor Al atoms. The increase in the optical band gap is explained by the BM effect in terms of increased carrier concentration [57]; the optical band gap widening for an n-type semiconductor with a parabolic band is given by:

$$\Delta E^{BM} = \frac{h^2}{8\pi^2 m^*}(3\pi^2 n)^{2/3} \tag{2}$$

where ΔE^{BM} is the blue shift in the optical band gap, h is Planck's constant, n is the carrier concentration, and m^* is the effective mass of the electrons in the conduction band [58]. The increase in optical band gap essentially increases the carrier concentration giving rise to increased sensing response. The results also imply that FSP-synthesized NPs exhibit larger optical band gaps.

Fig. 7 shows the adsorption-desorption isotherms of pure and Al-doped ZnO NPs synthesized by FSP and HT. The physisorption isotherms of undoped and Al-doped ZnO NPs synthesized by FSP (type III) are different from those in undoped and Al-doped ZnO NPs (type IV)

synthesized by HT, which is attributed to different porosities [62]. While the FSP-made ZnO particles possess only virtual macropores resulting from particle agglomeration, the HT-made ZnO particles exhibit mesoporous structures. An empirical classification of hysteresis loops [62] is given by IUPAC (International Union of Pure and applied Chemistry), in which the shape of the hysteresis loops (types H1 – H4) are correlated with the texture of adsorbent materials. All curves in Fig. 7 correspond to type H1. According to this classification, type H1 is often associated with porous materials exhibiting a narrow distribution of relatively uniform (cylindrical-like) pores [59]. The specific surface areas of the as-prepared pure and Al-doped ZnO NPs synthesized by HT are ~35 and ~42 m^2/g, respectively, while those made by FSP are ~44 and ~48 m^2/g, respectively. The surface areas of the Al-doped ZnO NPs are larger than those of the pure ZnO NPs that may result from the Al incorporation, as observed similarly for Si- [60] and Ti-doped NPs thermally stabilizing ZnO at smaller particle sizes [24].

Fig. 8 shows the sensing response, oxygen vacancies, optical band gaps, and BET specific surface areas of the pure and Al-doped ZnO NPs synthesized by FSP and HT. A noteworthy feature is that a remarkably enhanced response is observed in the Al-doped ZnO synthesized by FSP as compared to HT (Fig. 8a). The sensing responses of the Al-doped ZnO are ~245 (FSP) and ~56 (HT) to 10 ppm acetone at 450 °C. However, pure ZnO exhibited similar responses regardless of the synthesis method (~13 for FSP and ~11 for HT). This observation seems to be attributed primarily to the oxygen vacancy density that follows the same trend resulting in greater number of adsorbed oxygen ions on the surfaces of ZnO that can react with acetone [61].
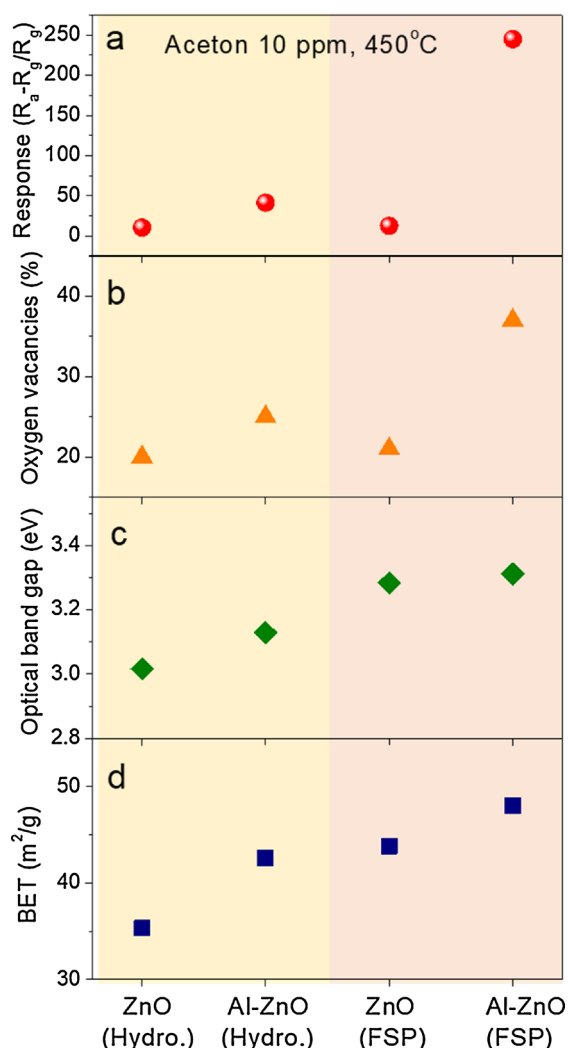
Fig. 8. Summary of the (a) sensing responses, (b) oxygen vacancies, (c) optical band gaps, and (d) BET surface areas of the pure and Al-doped ZnO NPs synthesized by FSP and HT.

4. Conclusions

We have investigated the acetone sensing properties of pure and Al-doped ZnO made by flame spray pyrolysis (FSP). Al-doped ZnO exhibited high sensing response of 245, response time of ~3 s and sensitivity of $S = 23\,ppm^{-1}$ for the detection of 10 ppm acetone at an optimum operational temperature of 450 °C. The FSP-made Al-doped ZnO showed better sensing properties than pure ZnO and when made by hydrothermal synthesis (*Response* = 56, response time ~12 s, and $S = 4$). Furthermore, the sensing response to 1 ppm acetone at 90% RH is superior to other chemoresistive acetone sensors and features competitive response time and lowest measured detection limit (100 ppb), attractive for breath analysis. The enhanced sensing properties of the Al-doped ZnO made by FSP are attributed primarily to a higher density of oxygen vacancies, higher carrier concentration and slightly larger specific surface area than that in Al-doped ZnO made by HT, giving rise to more oxygen ions that can react with acetone molecules. Therefore, the superior sensing performance of Al-doped ZnO made by FSP offers opportunities for a wide range of applications such as environmental and industrial monitoring systems as well as breath analyzers for monitoring personal health conditions.

Appendix A. Supplementary data

Supplementary material related to this article can be found, in the online version, at doi:https://doi.org/10.1016/j.snb.2018.12.001.

References

[1] M. Righettoni, A. Amann, S.E. Pratsinis, Breath analysis by nanostructured metal oxides as chemo-resistive gas sensors, Mater. Today 18 (2014) 163–171.
[2] M.P. Kalapos, On the mammalian acetone metabolism: from chemistry to clinical implications, Biochim. Biophys. Acta 1621 (2003) 122–139.
[3] A. Manolis, The diagnostic potential breath analysis, Clin. Chem. 29 (1983) 5–15.
[4] M. Statheropoulos, A. Agapiou, A. Georgiadou, Analysis of expired air of fasting male monks at Mount Athos, J. Chromatogr. B 823 (2006) 274–279.
[5] A.T. Güntner, N.A. Sievi, S.J. Theodore, T. Gulich, M. Kohler, S.E. Pratsinis, Noninvasive body fat burn monitoring from exhaled acetone with Si-doped WO_3-sensing nanoparticles, Anal. Chem. 89 (2017) 10578–10584.
[6] J.C. Anderson, W.J.E. Lamm, M.P. Hlastala, Measuring airway exchange of endogenous acetone using a single-exhalation breathing maneuver, J. Appl. Physiol. 100 (2006) 880–889.
[7] P. Spanel, K. Dryahina, A. Rejskova, T.W.E. Chippendale, D. Smithm, Breath acetone concentration; biological variability and the influence of diet, Physiol. Meas. 32 (2011) N23–N31.
[8] J.C. Anderson, Measuring breath acetone for monitoring fat loss: review, Obesity 23 (2015) 2327–2334.
[9] M. Phillips, Method for the collection and assay of volatile organic compounds in breath, Anal. Biochem. 247 (1997) 272–278.
[10] C. Turner, C. Walton, S. Hoashi, M. Evans, Breath acetone concentration decreases with blood glucose concentration in type I diabetes mellitus patients during hypoglycaemic clamps, J. Breath Res. 3 (2009) 046004.
[11] H. Lord, Y. Yu, A. Segal, J. Pawliszyn, Breath analysis and monitoring by membrane extraction with sorbent interface, Anal. Chem. 74 (2002) 5650–5657.
[12] K. Schwarz, A. Pizzini, B. Arendacka, K. Zerlauth, W. Filipiak, A. Schmid, A. Dzien, S. Neuner, M. Lechleitner, S. Scholl-burgi, Breath acetone—aspects of normal physiology related to age and gender as determined in a PTR-MS study, J. Breath Res. 3 (2009) 027003.
[13] A.T. Güntner, V. Koren, K. Chikkadi, M. Righettoni, S.E. Pratsinis, E-nose sensing of low-ppb formaldehyde in gas mixtures at high relative humidity for breath screening of lung cancer? ACS Sens. 1 (2016) 528–535.
[14] M. Righettoni, R. Alessandro, A.T. Güntner, C. Loccioni, S.E. Pratsinis, T.H. Risby, J. Breath Res. 9 (2015) 047101.
[15] L. Wang, A. Teleki, S.E. Pratsinis, P.I. Gouma, Ferroelectric WO3 nanoparticles for acetone selective detection, Chem. Mater. 20 (2008) 4794–4796.
[16] S. Singkammo, A. Wisitsoraat, C. Sriprachuabwong, A. Tuantranont, S. Phanichphant, C. Liewhiran, Electrolytically exfoliated graphene-loaded flame-made Ni-doped SnO2 composite film for acetone sensing, ACS Appl. Mater. Interfaces 7 (2015) 3077–3092.
[17] Z. Zhang, Z. Wen, Z. Yea, L. Zhu, Gas sensors based on ultrathin porous Co3O4 nanosheets to detect acetone at low temperature, RSC Adv. 5 (2015) 59976-56285.
[18] M.H. Darvishnejad, A.A. Firooz, J. Beheshtian, A.A. Khodadadi, Highly sensitive and selective ethanol and acetone gas sensors by adding some dopants (Mn, Fe, Co, Ni) onto hexagonal ZnO plates, RSC Adv. 6 (2016) 7838–7845.
[19] X. Zhou, B. Wang, H. Sun, C. Wang, P. Sun, X. Li, X. Hu, G. Lu, Template-free synthesis of hierarchical ZnFe2O4 yolk–shell microspheres for high-sensitivity acetone sensors, Nanoscale 8 (2016) 5446–5453.
[20] V.K. Tomer, K. Singh, H. Kaur, M. Shorie, P. Sabherwal, Rapid acetone detection using indium loaded WO3/SnO2 nanohybrid sensor, Sens. Actuators B: Chem. 253 (2017) 703–713.
[21] R. Malik, V.K. Tomer, L. Kienle, V. Chaudhary, S. Nehra, S. Duhan, Ordered mesoporous Ag–ZnO@g-CN nanohybrid as highly efficient bifunctional sensing material, Adv. Mater. Interfaces 5 (8) (2018) 1701357.
[22] V.K. Tomer, R. Malik, K. Kailasam, Near-room-temperature ethanol detection using Ag-loaded mesoporous carbon nitrides, ACS Omega 2 (2017) 3658–3668.
[23] N.H. Al-Hardan, M.J. Abdullah, A.A. Aziz, H. Ahmad, L.Y. Low, ZnO thin films for VOC sensing applications, Vacuum 85 (2010) 101–106.
[24] A.T. Güntner, N.J. Pineau, D. Chie, F. Krumeich, S.E. Pratsinis, Selective sensing of isoprene by Ti-doped ZnO for breath diagnostics, J. Mater. Chem. B 4 (2016) 5358–5366.
[25] Q. Yuan, Y.P. Zhao, L. Li, T. Wang, Ab initio study of ZnO-based gas-sensing mechanisms: surface reconstruction and charge transfer, J. Phys. Chem. C 113 (2009)

6107–6113.

[26] S.J. Chang, T.J. Hsueh, I. Chen, S.F. Hsieh, S.P. Chang, C.L. Hsu, Highly sensitive ZnO nanowire acetone vapor sensor with Au adsorption, IEEE Trans. Nanotechnol. 7 (2008) 754–759.

[27] N.L. Hadipour, A. Ahmadi Peyghan, H. Soleymanabadi, Theoretical study on the Al-doped ZnO nanoclusters for CO chemical sensors, J. Phys. Chem. C 119 (2015) 6398–6404.

[28] L. Mädler, H.K. Kammler, R. Mueller, S.E. Pratsinis, Controlled synthesis of na-nostructured particles by flame spray pyrolysis, J. Aerosol Sci. 33 (2002) 369–389.

[29] L.N. Dem'yanets, V.I. Lyutin, Status of hydrothermal growth of bulk ZnO: latest issues and advantages, J. Cryst. Growth 310 (2008) 993–999.

[30] A.J. Gröhn, S.E. Pratsinis, A.S. Ferrer, R. Mezzenga, K. Wegner, Scale-up of nano-particle synthesis by flame spray pyrolysis: the high-temperature particle residence time, Ind. Eng. Chem. Res. 53 (26) (2014) 10734–10742.

[31] S. Kuhne, M. Graf, A. Tricoli, F. Mayer, S.E. Pratsinis, A. Hierlemann, Wafer-level flame-spray-pyrolysis deposition of gas-sensitive layers on microsensors, J. Micromech. Microeng. 18 (2008) 035040.

[32] Oliver Waser, Oliver Brenner, ArtoJ. Groehn, Sotiris E. Pratsinis, Process design for size-controlled flame spray synthesis of $Li_4Ti_5O_{12}$ and electrochemical performance, Chem. Process. Eng. 38 (1) (2017) 51–66.

[33] A.T. Güntner, M. Righettoni, S.E. Pratsinis, Selective sensing of NH3 by Si-doped α-MoO_3 for breath analysis, Sens. Actuators B: Chem. 223 (2016) 266–273.

[34] A.T. Güntner, N.J. Pineau, P. Mochalski, H. Wiesenhofer, A. Agapiou, C.A. Mayhew, S.E. Pratsinis, Sniffing entrapped humans with sensor arrays, Anal. Chem. 90 (8) (2018) 4940–4945.

[35] L. Mädler, W.J. Stark, S.E. Pratsinis, Flame-made ceria nanoparticles, J. Mater. Res. 17 (2002) 1356–1362.

[36] R. Yoo, S. Cho, M.-J. Song, W. Lee, Highly sensitive gas sensor based on Al-doped ZnO nanoparticles fordetection of dimethyl methylphosphonate as a chemical warfareagent simulant, Sens. Actuators B: Chem. 221 (2015) 217–223.

[37] R. Yoo, D. Lee, S. Cho, W. Lee, Al doping effect on sensing properties of ZnO na-noparticles for detection of 2-chloroethyl ethylsulfide as a mustard simulant, Sens. Actuators B: Chem. 254 (2018) 1242–1248.

[38] R. Strobel, S.E. Pratsinis, Flame aerosol synthesis of smart nanostructured materials, J. Mater. Chem. 17 (2007) 4743–4756.

[39] T. Tani, L. Mädler, S.E. Pratsinis, Homogeneous ZnO nanoparticles by flame spray pyrolysis, J. Nanopart. Res. 4 (2002) 337–343.

[40] R.D. Shannon, Revised effective ionic radii and systematic studies of interatomic distances in halides and chalcogenides, Acta Cryst. (1976) 751–767.

[41] L.-J. Bie, X.-N. Yan, J. Yin, Y.-Q. Duan, Z.-H. Yuan, Nanopillar ZnO gas sensor for hydrogen and ethanol, Sens. Actuators B: Chem. 126 (2007) 604–608.

[42] T.H. Risby, S.F. Solga, Current status of clinical breath analysis, Appl. Phys. B: Lasers Opt. 85 (2 − 3) (2006) 421–426.

[43] L. Ferrus, H. Guenard, G. Vardon, P. Varene, Respiratory water loss, Respir. Physiol. 39 (1980) 367–381.

[44] M. Righettoni, A. Tricoli, S.E. Pratsinis, Si:WO_3 sensors for highly selective detec-tion of acetone for easy diagnosis of diabetes by breath analysis, Anal. Chem. 82 (2010) 3581–3587.

[45] S.-J. Choi, C. Choi, S.-J. Kim, H.-J. Cho, S. Jeon, I.-D. Kim, Facile synthesis of hierarchical porous WO_3 nanofibers having 1D nanoneedles and their

functionalization with non-oxidized graphene flakes for selective detection of acetone molecules, RSC Adv. 5 (2015) 7584–7588.

[46] K.-I. Choi, S.-J. Hwang, Z. Dai, Y.C. Kang, J.-H. Lee, Rh-catalyzed WO_3 with anomalous humidity dependence of gas sensing characteristics, RSC Adv. 4 (2014) 53130–53136.

[47] S.-J. Choi, B.-H. Jang, S.-J. Lee, B.K. Min, A. Rothschild, I.-D. Kim, Selective de-tection of acetone and hydrogen sulfide for the diagnosis of diabetes and halitosis using SnO_2 nanofibers functionalized with reduced graphene oxide nanosheets, ACS Appl. Mater. Interf. 6 (2014) 2588–2597.

[48] W. Li, Z. Feng, E. Dai, J. Xu, G. Bai, Organic vapour sensing properties of area-ordered and size-controlled silicon nanopillar, Sensors 16 (2016) 1880–1887.

[49] J.T. Chen, J. Wang, R.F. Zhuo, D. Yan, J.J. Feng, F. Zhang, P.X. Yan, The effect of Al doping on the morphology and optical property of ZnO nanostructures prepared by hydrothermal process, Appl. Surf. Sci. 255 (2009) 3959–3964.

[50] R. Sankar Ganesh, M. Navaneethan, Ganesh Kumar Mani, S. Ponnusamy, K. Tsuchiya, C. Muthamizhchelvan, S. Kawasaki, Y. Hayakawa, Influence of Al doping on the structural, morphological, optical, and gas sensing properties of ZnO nanorods, J. Alloys. Compd. 698 (2017) 555–564.

[51] J. Wang, Y. Li, Y. Kong, J. Zhou, J. Wu, X. Wu, W. Qin, Z. Jiao, L. Jiang, Non-fluorinated superhydrophobic and micro/nano hierarchical Al doped ZnO film: the effect of Al doping on morphological and hydrophobic properties, RSC Adv. 5 (2015) 81024–81029.

[52] X. Li, Y. Wang, W. Liu, G. Jiang, C. Zhu, Study of oxygen vacancies' influence on the lattice parameter in ZnO thin film, Mater. Lett. 85 (2012) 25–28.

[53] B.E. Sernelius, K.F. Berggren, Z.C. Jin, I. Hamberg, C.G. Granqvist, Band-gap tai-loring of ZnO by means of heavy Al doping, Phys. Rev. B 37 (1988) 10244–10248.

[54] S. Suwanboon, P. Amornpitoksuk, A. Sukolrat, Dependence of optical properties on doping metal, crystallite size and defect concentration of M-doped ZnO nano-powders (M = Al, Mg, Ti), Ceram. Int. 37 (2011) 1359–1365.

[55] J. Tauc, Amorphous and Liquid Semiconductors, Plenum Press, New York, 1974 p. 171.

[56] R.S. Weber, Effect of local structure on the UV-visible absorption edges of mo-lybdenum oxide clusters and supported molybdenum oxide, J. Catal. 151 (1995) 470–474.

[57] C.E. Kim, P. Moon, S. Kim, J.-M. Myoung, H.W. Jang, J. Bang, I. Yun, Effect of carrier concentration on optical bandgap shift in ZnO:Ga thin films, Thin Solid Films 518 (2010) 6304–6307.

[58] I. Hamberg, C.G. Granqvist, K.-F. Berggren, B.E. Sernelius, L. Engström, Band-gap widening in heavily Sn-doped In_2O_3, Phys. Rev. B 30 (1984) 3240–3249.

[59] M. Thommes, Physical adsorption characterization of nanoporous materials, Characterization of nanoporous materials, Chemie Ingenieur Technik 82 (7) (2010) 1059–1073.

[60] L. Madler, W.J. Stark, S.E. Pratsinis, Rapid synthesis of stable ZnO quantum dots, J. Appl. Phys. 92 (2002) 6537–6540.

[61] M. Epifani, J. Daniel Prades, E. Comini, E. Pellicer, M. Avella, P. Siciliano, G. Faglia, A. Cirera, R. Scotti, F. Morazzoni, J. Ramon Morante, J. Phys. Chem. C 112 (2008) 19540–19546.

[62] K.S.W. Sing, D.H. Everett, R.A.W. Haul, L. Moscou, R.A. Pierotti, J. Rouquerol, T. Siemieniewka, Pure Appl. Chem. 57 (1985) 609–619.